Thickness and cavitation effects on vibrations of hydrofoils at large angle of attack

Christophe Sarraf, Henda Djeridi, Jean-Yves Billard

Thickness and cavitation effects on vibrations of hydrofoils at large angle of attack

Christophe Sarraf, Henda Djeridi, and Jean-Yves Billard

Institut de Recherche de l'Ecole navale (IRENav), BP 600 Lanvéoc Poulmic, 29240 BREST ARMEES, France, billard@ecole-navale.fr

1 Introduction

One of the main interest of thick hydrofoils is the stall delay that such profiles can provide when used at high incidences. In naval applications such profiles are use for the design of rudders or POD struts. In spite of their increasing use their behavior is not clearly understood and very few data are available concerning their hydrodynamic behavior at low and high incidences (turbulent boundary layer structures, performance control, unsteady separated flows, cavitating behavior or bucket and induced vibrations). In order to get some insight, an experimental study on the hydrodynamic and cavitating behaviour of 2D Naca (15, 25, 35%) symmetric hydrofoils at moderate chord Reynolds numbers ($\approx 0.5 \times 10^6$) is performed.

2 Experimental set up and measurements

The experiments have been conducted in the hydrodynamic tunnel of the French Naval Academy. This facility is fitted with a 1 m long and 0.192×0.192 m^2 square cross test section, in which a maximum velocity of 15ms^{-1} can be achieved. The turbulence intensity upstream at the entrance of the test section is 2 %. The three designed, two dimensional, Naca four digits foils have a symmetric mean line with relative maximum thickness of 15%, 25%, 35% located at 25% from the leading edge. The experiments have been performed on 100 mm chord length and 192 mm span length hydrofoils for a range of Reynolds number based on the chord length of $0.5 \times 10^6 < \mathrm{Re} < 1.3 \times 10^6$. The blockage ratios defined as t/H (H is the height of the test section, and t the maximum thickness of the foil are respectively 0.078 for the Naca0015 and 0.182 for the Naca0035. The draft of the experimental configuration is shown on Figure 1.

Lift and drag measurements have been performed using a resistive gauge hydrodynamic balance calibrated in our laboratory. The mean and rms values

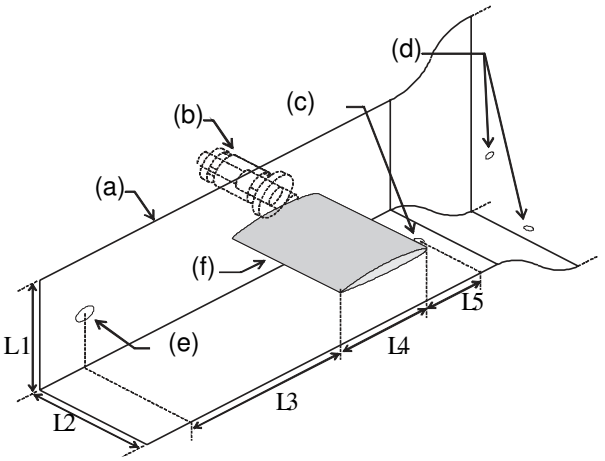

Fig. 1. Experimental set up:
(a) back wall of the vein
(b) force balance
(c) downstream pressure tap
(d) upstream pressure taps
(e) acoustical pressure sensor
(f) profile
L1 = L2 = 192 mm
L3 = 135 mm
L4 = 100 mm
L5 = 225 mm

have been estimated from 30 s test measurements realized at 1830 Hz. The determination of hydrodynamic parameters has been performed for $0°<\alpha<35°$ and the maximum range for the balance is 0-180 daN for the lift and 0-17 daN for the drag force.
Dynamic pressure measurements have been realized using a PCB 106B50 transducer located 3 chords downstream of the foil trailing edge when this one has an 0° angle of attack. Vertically the foil is in the middle of the test section. Acquisition of the pressure signal is realized using a VXI digital system.
Velocity measurements have been realized using a DANTEC, three beams, two components LDV system operated in back scatering mode. The mean and fluctuating parts of the velocity, as well as the signal time-histories have been measured. The flow was seeded with Iriodin particules. A particular attention has been paid to the quality of the data rate that remained larger than 2 kHz but very near the profile where it was difficult to raised over 300 Hz. Velocity spectrum presented have been realized in high data rate conditions.

3 Thickness effects

3.1 Global parameters

Lift and drag

Lift and drag, figure 2 and 3, behave classically for low angles of attack.
An abrupt loss of lift, characteristic of the stall, is observed on the Naca0015 and on Naca0025 for higher angles. For the 2 thinnest profiles the lift behaviour is linear for small values of the angle of attack. For the thickest one, a screen effect delays the establishment of the lift, leading to a non linear behaviour for small angles of attack indicated by the black arrow on the figure 2. In the linear range of lift evolution the slope

$$\frac{dC_l}{d\alpha}$$

decreases with increasing thickness. This behavior is characteristic of thick profiles. It can be noticed that the linear range of angles of attack increases with the thickness of the profile. Stall appears for angles of 13°, 23° and 35°respectively on Naca0015, 0025 and 0035.
The evolution of the drag coefficient remains classical, figure 3:

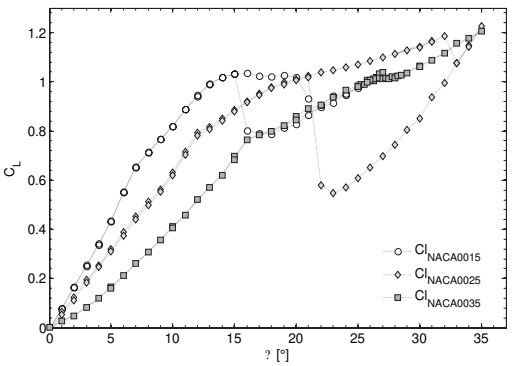

Fig. 2. Lift coefficients for the three profiles

- For low incidences the effect of thickness is characterized by an increase of the drag coefficient with increasing thickness ;
- For the two thinest profiles a classical behavior with drag proportional to the square of the angle of attack is observed and an abrupt increase of drag is observed at stall occurence ;
- The thickest profile behaves quite differently with a decrease of the parabola coefficient for $\alpha = 27$ °.

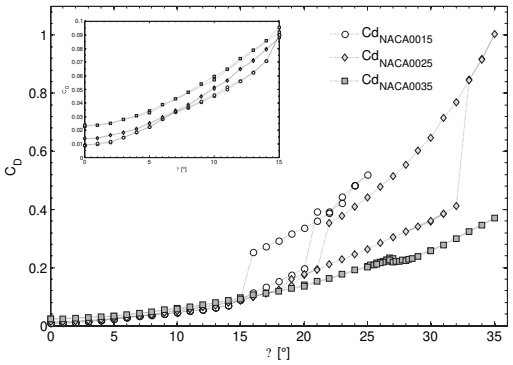

Fig. 3. Drag coefficients for the three profiles. Inserted figure is a magnification for low angle values.

Shape factor at 10° angle of attack

Measurements are carried out on lines normal to the hydrofoil surface for different positions x/c spaced of 10%, figure 4 and concern two components (normal and tangential) of the velocity and their fluctuations.

Velocity profiles were numerically integrated to compute the displacement,

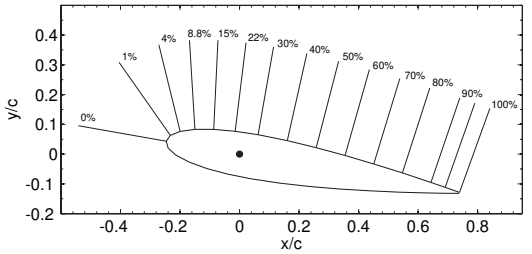

Fig. 4. Measuring grid along normals on the Naca0015 hydrofoil

$\delta 1$, momentum, $\delta 2$ and energy, $\delta 3$, thicknesses from which shape factors H_{12} and H_{23} are deduced. The following formulas are applied:

$$\delta_1 = \int_0^\delta \left(1 - \frac{u}{U_e}\right) dy,\ \delta_2 = \int_0^\delta \left(1 - \frac{u}{U_e}\right) \frac{u}{U_e} dy,\ \delta_3 = \int_0^\delta \left(1 - \frac{u^2}{U_e^2}\right) \frac{u}{U_e} dy$$

$$H_{12} = \frac{\delta_1}{\delta_2},\ H_{23} = \frac{\delta_2}{\delta_3}$$

U_e represents the external velocity on the normal line. In our case this velocity is the maximum velocity measured at the location. It can be observed on figure

5 that the thickness effect is associated with an increase of the length of the laminar region near the leading edge which grows from less than 10% on the Naca0015 to 30% on the Naca0035. At the end of this area the shape factor increases to reach a value of 3 to 4 just before the occurrence of the transition. After the transition, the value of H_{12} remains constant and equal to 1.6. This value increases near the trailing edge when the flow reaches conditions of separation. The constant value of H_{12} is larger than the value generally observed for turbulent boundary layers (1.4). From this figure it can be seen that the length of the laminar area at the leading edge of the profile increases with the thickness and that the turbulent boundary layer reaches detachment condition at the trailing edge of the thickest profile. It has been verified that the

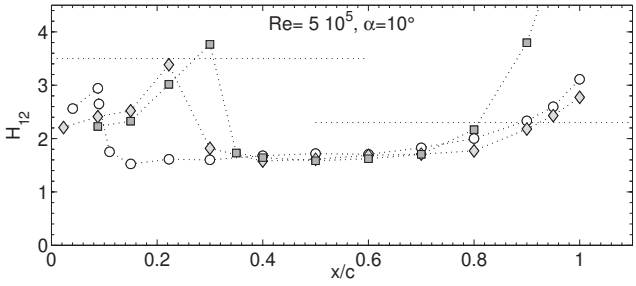

Fig. 5. Shape factors on the three profiles, ○ Naca0015, ◇ Naca0025, □ Naca0035

boundary layer with adverse pressure gradient verifies the correlation between H_{12} and H_{23} proposed by Truckenbrot and reported by Schlichting [1].

Noise level

Sound pressure levels have been determined by integration of the noise measurements realized in the wake of the profile. It can be seen from figure 6 that at low incidences the sound pressure level increases slightly with the thickness of the foil. Nevertheless the order of magnitude remains the same and for high incidences the differences between the three foils remains inside experimental errors.
For non cavitating conditions it can be noticed that:

- The thickness of the profile induces a slight increase of the SPL at low angle of attack.
- A decrease of the SPL can be observed on the three profiles at an incidence corresponding to the end of linear part of the lift coefficient curve.
- Then a sharp increase of the SPL can be observed on the 2 thinnest profiles when stall occurs.

The stall angle is too high on the thicker profile to allow, due to blockage effect, accurate measurements.

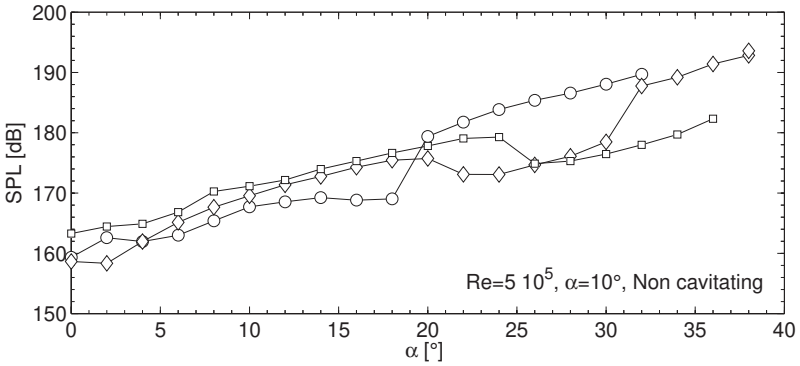

Fig. 6. Evolution of the sound pressure level on the three profiles with angle of attack, ○ Naca0015, ◇ Naca0025, □ Naca0035

3.2 Unsteady separated flow and high incidence

Spectral analysis and Strouhal number

From velocity measurements realized in the near wake of the profile at different incidences energy spectrum of the velocity fluctuations have been computed. The spectrums are presented on figure 7. From these figures it can be seen that a spectral frequency can be easily identify especially at high incidences where spectral harmonics appear on the spectrum.

When these frequencies are reported in a non dimensional manner as Strouhal numbers computed using the projected area of the profile, it can be noticed, figure 8, that for the higher incidences the classical value of 0.2 characteristic of Von Karman instability is achieved.

More interesting is the fact that for incidences comprised between 25 and 33° the two thicker profiles have a Strouhal number of 0.25 that falls to 0.2 at stall when the detachment point migrates violently from the suction side to the leading edge of the foil. On this figure velocities are corrected to take the blockage effect into account.

4 Cavitation effects

4.1 Global parameters

The cavitation development is characterized by use of the cavitating index classically defined by:

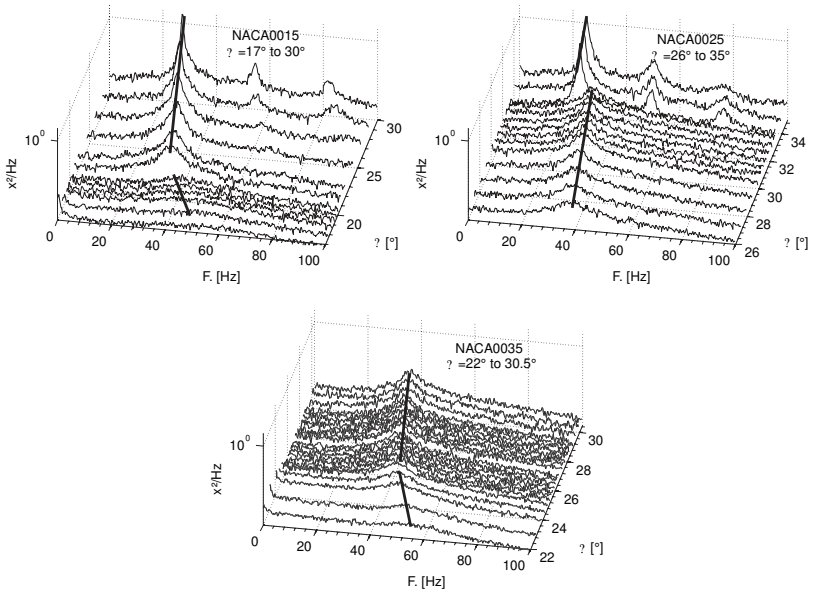

Fig. 7. Velocity spectrum in the near wake of the three profiles, (a) Naca0015, (b) Naca0025 and (c) Naca0035 for same flow conditions

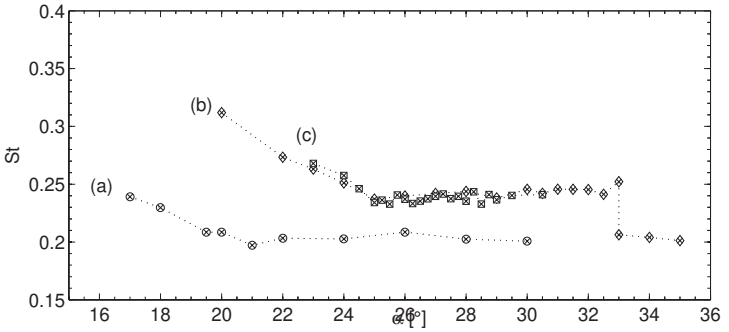

Fig. 8. Strouhal numbers (a - Naca0015, b - Naca0025, c - Naca0035)

$$\sigma = \frac{P_{ref} - P_v}{\frac{1}{2}\rho V_{ref}^2}$$

Cavitation bucket

The curves of incipient cavitation are reported on figure 9 for the three profiles. The experimental data are reported with the curves of minimum pressure coefficient, Cpmin. A good agreement could be observed for the three profiles with little scattering of experimental points.

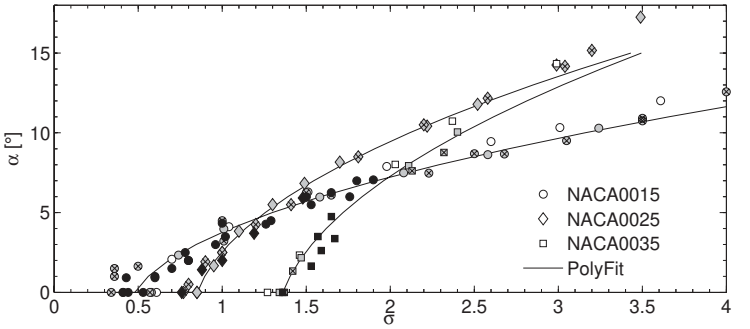

Fig. 9. Cavitation buckets on the three profiles

Cavitation development

For conditions corresponding to Re = 8×10^5, $\sigma = 2.35$ and $\alpha = 10°$a partial cavity is present on the 3 profiles but its development is not the same. A rather bi dimensional stable cavity is present on the thinner profile [2], a bi dimensional pulsating cavity is visible on the medium profile and a tri dimensional unstable cavity affects the thicker profile. Dynamic of such partial cavities has been described by Leroux et al. [3].
The distance between the leading edge and the sheet detachment increases with the thickness of the profile. The table 1 summaries the cavitating conditions.
Boundary layer measurements have been realized on the thinnest profile with and without sheet cavity. In the first case there is no indication for the existence of a laminar bubble but with the sheet cavity the increase of the sape factor in front of the cavity indicates that the separation of the laminar boudary layer is consecutive to the existence of the cavity, figure 10. These tests have not been realized yet on the two thickest profiles.

Table 1. Properties of sheet cavities on the three profiles

Profile	Detachment point	Length of the cavity
Naca0015	8 %	8 %
Naca0025	16 %	28 %
Naca0035	21 %	20 %

Noise level

For two different cavitation indexes noise measurements have been performed and reported on figure 11. The development of the cavity is associated

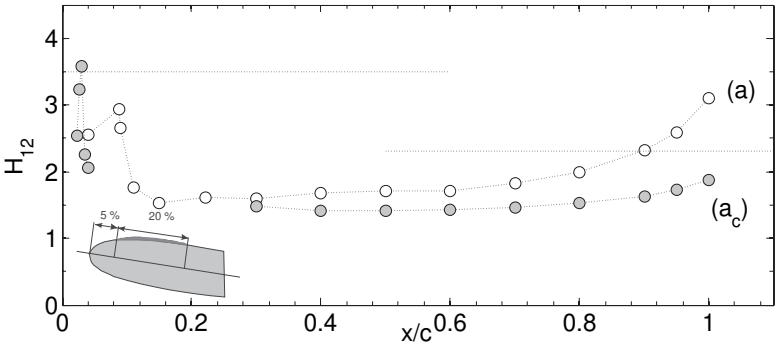

Fig. 10. Shape factor on NACA0015, 5°, cavitating and non cavitating conditions

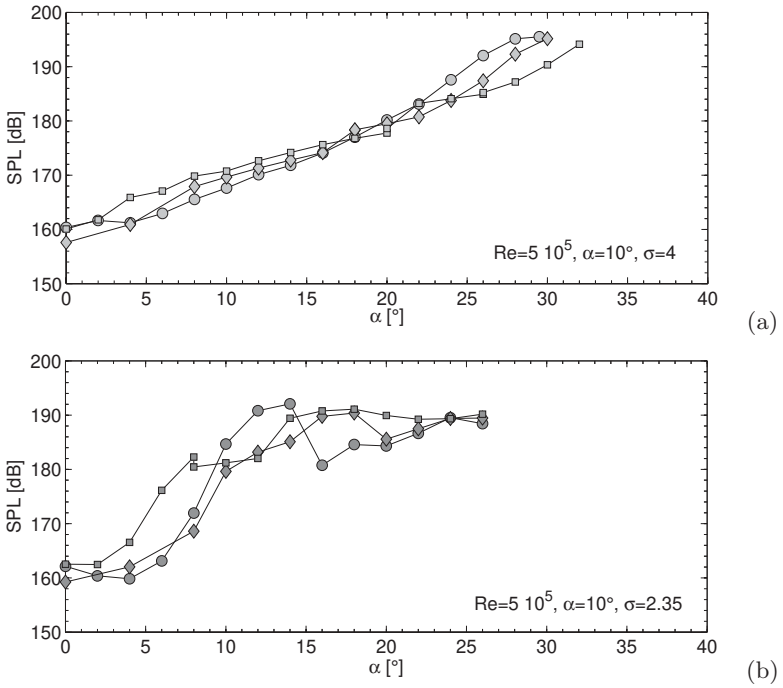

Fig. 11. Sound pressure level on the 3 profiles in different conditions, (a) $\sigma = 4$, (b) $\sigma = 2.35$

with an increase of the noise level for flow conditions where, in the non cavitating case, no vortex shedding is observed. The spectral analysis shows that the reduced frequencies correspond to a Strouhal number of 0.31 associated with the dynamic of the partial cavity (corresponding

low frequencies can be observed on figure 14 for angle of attacks comprised between 10 °and 20 °). Measurements can be detailed in the following manner:

- For moderate cavitation number, figure 11 a, the SPL is not strongly modified by cavitation even if a slight increase can be mentioned. The three curves evolve linearly and the thickness does not modify the noise level. We can point the disappearance of the slight decreased observed at the end of the linear part of the lift coefficient curve.
- For lower cavitation number, figure 11 b, the classical shape of the SPL curve is achieved with a sharp increase of SPL corresponding to the appearance of sheet cavity instabilities and a saturation corresponding to super cavitating conditions.

4.2 Unsteady cavitating separated flow

Spectral analysis

This part is devoted to the cavitation effects on the establishment and development of the von Karman street at high angle of attack. When incidence is increased, an organized motion due to the regular vortex shedding appears without cavitation. When cavitation appears the effect of entrained bubbles or pulsated cavities on the structure of the vortex shedding is studied using spectral analysis. Evolutions with angle of attack of the noise spectra on the three profiles are reported figure 12 13 and 14. For non cavitating conditions it can be seen on the three profiles that a spectral content corresponding to a Strouhal number of 0.2 emerges from the spectra. The vortex shedding is captured by the transducer in the wake, but compared to the spectrum obtained using LDV, figure 7, the peak value is less pronounced. This is due to the different locations of measurements. Indeed, the vortex shedding is more evident in the shear layer near the trailing edge. It can be noticed that the two states of the flow characterized by two values of St (0.25 in state I and 0.2 in state II) disappears with the developed cavitation. [4].
The cavitation impacts the partially attached flow at the leading edge and modifies the location of the detachment point. The non linear interaction between Kelvin Helmotz and Karman instabilities is no more responsible of the establishment of two flow states, the sheet closure instability is predominant. For lower cavitation numbers an impact of sheet pulsation at lower frequencies (f = 12 Hz) corresponding to lower Strouhal numbers characteristic of sheet closure instabilities inhibates the establishment of Karman instability. This phenomenon can be observed on the three profiles on figures 12, 13 and 14. For the lower cavitation number the establishment of a super cavity can be observed in correlation with the disappearance of all the spectral frequencies at high incidences.

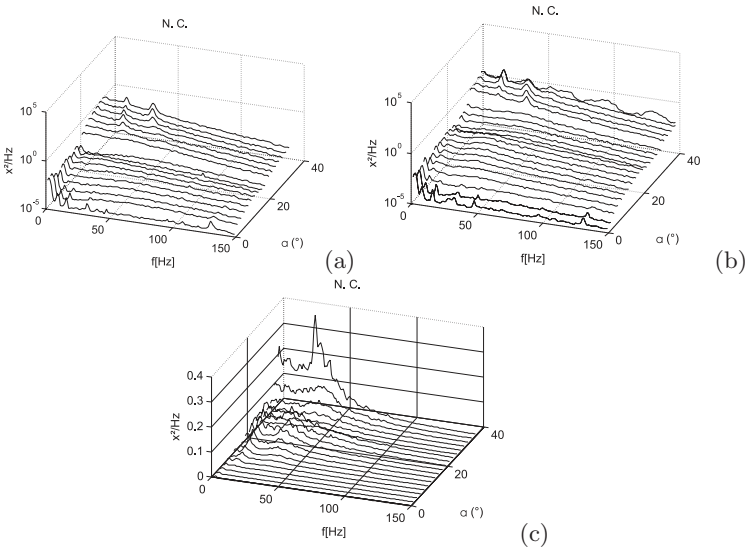

Fig. 12. Noise spectra for the 3 profiles in same conditions, (a) Naca0015, (b) Naca0025 and (c) Naca0035, non cavitating conditions

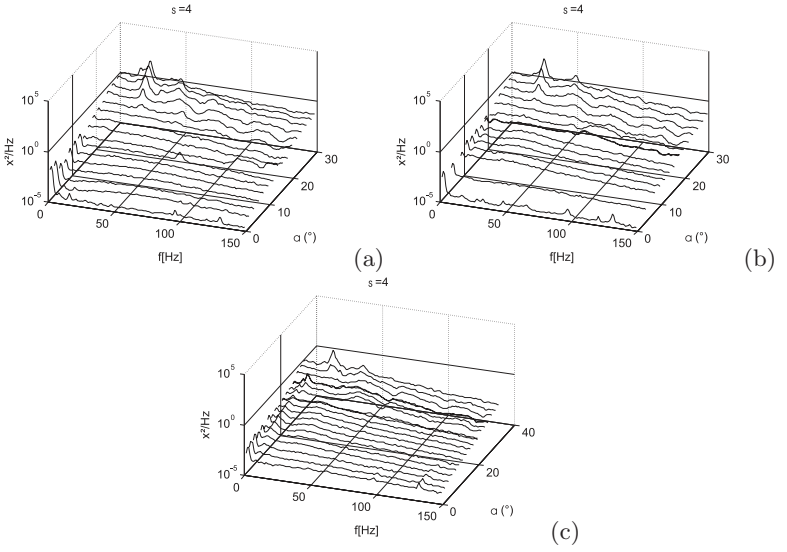

Fig. 13. Noise spectra for the 3 profiles in same conditions, (a) Naca0015, (b) Naca0025 and (c) Naca0035, $\sigma = 4$

5 Conclusion

The global steady and unsteady performances of 3 Naca symmetrical profiles have been measured. At stall hysteretic behaviour and unsteady evolution

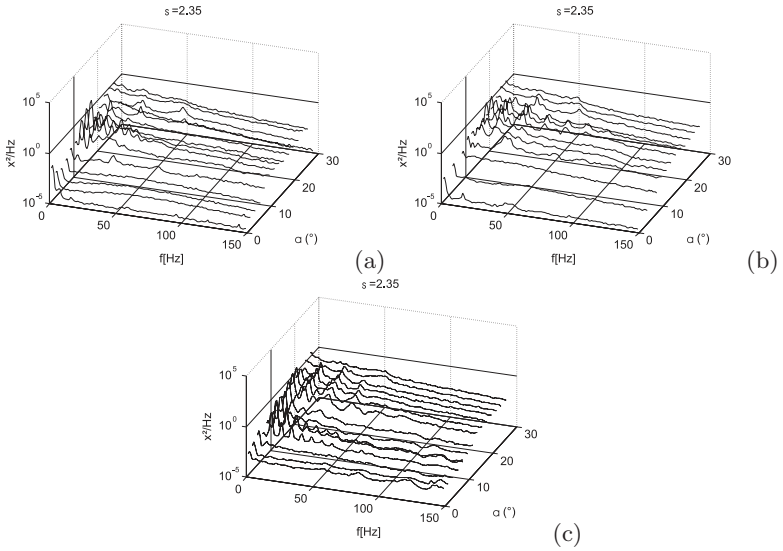

Fig. 14. Noise spectra for the 3 profiles in same conditions, (a) Naca0015, (b) Naca0025 and (c) Naca0035, $\sigma = 2.35$

of characteristics are described. For the same conditions the cavitating behaviour is described and the noise associated with the partial cavity is analysed showing that complex interactions between the flow and cavity dynamics will occur.

References

1. Schlichting H., Kestin J. (1979) , Boundary layer theory, 7th edition, Science/Engineering/Math, McGraw-Hill.
2. Sarraf, C., Ait Bouziad, Y., Djeridi, H., Farhat, M., Billard, J-Y. (2006) Effect of cavitation on the structure of the boundary layer in the wake of a partial cavity International symposium on cavitation, CAV2006, 11-15 september, Wageningen, The Netherlands.
3. Leroux, J.B., Astolfi, J.A., Billard, J.Y. (2004) Jounal of fluids engineering, vol 126: 94-101
4. Sarraf, Djeridi, H., Billard, J-Y. (2007) Effect of cavitation on the structure of the boundary layer in the wake of a partial cavity International symposium on cavitation, IUTAM Symposium - Unsteady Separated Flows and their Control, 18-22 June, Corfu, Greece.